PAPER

Centralized Inter-Cell Interference Coordination Using Multi-Band 3D Beam-Switching in Cellular Networks

Hiroyuki SEKI[†a)], ***Senior Member and*** **Fumiyuki ADACHI**[††], ***Fellow***

SUMMARY The deployment of small cells is one of the most effective means to cope with the traffic explosion of cellular mobile systems. However, a small cell system increases the inter-cell interference, which limits the capacity and degrades the cell-edge user throughput. Inter-cell interference coordination (ICIC), such as fractional frequency reuse (FFR), is a well-known scheme that autonomously mitigates inter-cell interference. In the Long Term Evolution (LTE)-Advanced, the three-dimensional (3D) beamforming, which combines conventional horizontal beamforming and vertical beamforming, has been gaining increasing attention. This paper proposes a novel centralized ICIC scheme that controls the direction of narrow 3D beam for each frequency band of each base station. The centralized controller collects information from the base stations and calculates sub-optimum combinations of narrow beams so as to maximize the proportional fair (PF) utility of all users. This paper describes the throughput of the new centralized ICIC scheme as evaluated by computer simulations and shows it has a significant gain in both average user throughput and cell-edge user throughput compared with the conventional ICIC scheme. This paper also investigates the feasibility of the scheme by assessing its throughput performance in a realistic deployment scenario.
key words: *inter-cell interference coordination, 3D beam-switching, PF utility, KKT algorithm, spatial user multiplexing*

1. Introduction

The amount of data traffic is explosively growing in cellular mobile systems because of the increase in video traffic and the spread of smartphones. Annual growth rates of more than 60% have been reported recently [1]. Future mobile systems, such as fifth generation cellular mobile systems (5G), are expected to handle more than 1,000 times the data traffic of today [2]. There are three important means to cope with this traffic explosion: (a) spectrum efficiency improvement, (b) bandwidth extension, and (c) small cell deployment. Higher spectrum efficiency can be achieved by using multiple input multiple output (MIMO) technology enhancement and by adopting new radio access technologies. In order to extend the bandwidth, the utilization of higher frequency spectrum, such as millimeter wavelengths, should be considered. On the other hand, deployment of small cells is the most effective way to increase the capacity per unit area and it can be realized by simply decreasing the cell radius of the conventional macrocell. However, shortening the inter-site distance (ISD) changes the cell capacity from noise-limited to interference-limited because of the increased inter-cell interference. The increase in inter-cell interference would also degrade cell-edge user throughput. Inter-cell interference coordination (ICIC), such as fractional frequency reuse (FFR), has been investigated as a way to improve cell-edge user throughput [3]–[5]. To realize an autonomous form of ICIC, information about the frequency bands causing strong interference in other cells must be exchanged among neighbor base stations through an inter-site interface (X2-interface) specified in the Long Term Evolution (LTE) [6].

In the ICIC scheme using FFR, the transmission power of the "cell-edge user band", which is a portion of the system frequency band, is set higher than the rest of frequency bands so as to increase the desired signal power of cell-edge users without increasing the inter-cell interference. In another ICIC scheme, the antenna tilt angle is controlled to reduce the inter-cell interference. The antenna tilt angle of the cell-edge user band is set smaller than those of the other frequency bands [7]. However, these conventional ICIC schemes improve the cell-edge user throughput at the expense of the overall throughput. Therefore, a new ICIC scheme is desirable, i.e., one that greatly improves both the average user throughput and the cell-edge user throughput.

In LTE-Advanced, three-dimensional (3D) beamforming techniques which exploit the degrees of freedom in the vertical direction of array antenna are investigated to reduce the inter-cell interference and enhance the capacity [8]–[10]. The user specific dynamic beamforming was studied in [8], [9], and the vertical sectorization considering the load-balancing was studied in [10]. However, previous works did not incorporate 3D beamforming with ICIC.

This paper proposes a novel ICIC scheme that controls narrow 3D beams in order to reduce the inter-cell interference and greatly improve throughput performance in comparison with the conventional ICIC scheme using wide beam sector antennas. The proposed scheme uses multiple bands, and the direction of the narrow beam associated with each band is designed to be switched independently to cover the whole macrocell (sector). Our scheme uses a centralized controller to coordinate the directions of the narrow beam of each band of all controlled base stations for downlink transmissions. Therefore, the centralized controller needs to collect information, such as the received signal strength, via feedback from the user equipment (UE). The centralized controller calculates the downlink signal-

Manuscript received September 30, 2014.
Manuscript revised February 14, 2015.
[†]The author is with Fujitsu Laboratories Ltd., Kawasaki-shi, 213-0012 Japan.
[††]The author is with the Department of Communications Engineering, Graduate School of Engineering, Tohoku University, Sendai-shi, 980-8579 Japan.
a) E-mail: hseki@jp.fujitsu.com
DOI: 10.1587/transcom.E98.B.1363

to-interference plus noise power ratio (SINR) of all users for all possible combinations of narrow beams. After that, it calculates the expected user throughput under the assumption of proportional fair (PF) scheduling by using our previously proposed centralized resource allocation method [11]. Convex optimization using the Karush-Kuhn-Tucker (KKT) condition is applied to find the resource allocation ratio that enables the user throughput to be estimated. It then calculates sub-optimum combinations of narrow beams so as to maximize the PF utility of all users. Moreover, our scheme executes spatial user multiplexing by assigning up to two different narrow beams to the same frequency band in order to achieve the enhanced throughput.

In this paper, we evaluate the throughput performance of our centralized ICIC scheme via computer simulation. Since our scheme can be applied to the conventional macrocells, the performance of conventional ICIC is also evaluated for comparison. In addition, we demonstrate the feasibility of our scheme by investigating the effect of varying the measurement threshold and user mobility and the existence of uncontrolled base stations.

The rest of the paper is organized as follows. Section 2 explains our system model. Section 3 gives a detailed explanation of the proposed algorithm. Section 4 presents the evaluation of the throughput using computer simulations. Section 5 concludes the paper.

2. System Model

This section explains the system model of our centralized ICIC and that of the conventional FFR. It also explains the configuration of multi-band 3D beam-switching and the details of the 3D beam patterns used in our scheme. The simulation parameters are also described in this section.

2.1 Cell Layout and Basic Simulation Parameters

In this paper, we shall deal with the downlink of an LTE-Advanced system. We assume a macrocell layout with an ISD of 500 m; i.e., the cell radius is relatively small, and the capacity is interference-limited. The multi-cell structure is outlined in Fig. 1. There are seven cell sites with three sectors per site, and the wrap-around technique [12] is used to calculate the inter-cell interference at each cell. The simulation parameters are based on the 3GPP simulation model [13], and the assumptions used in our simulation are summarized in Table 1. The antenna pattern of the base station (BS) is also described in the table. For the conventional macrocell, the horizontal beamwidth φ_{3dB} is set to 70 degrees, and the azimuth angle $\varphi_{azimuth}$ is set to 0 degrees. An antenna down tilt θ_{tilt} of 15 degrees is recommended for an ISD of 500 m [13]. The system bandwidth of 10 MHz is equally divided under the assumption that there are multiple frequency bands in the simulation.

The SINR of UE #n in band #k of macrocell #j is calculated as

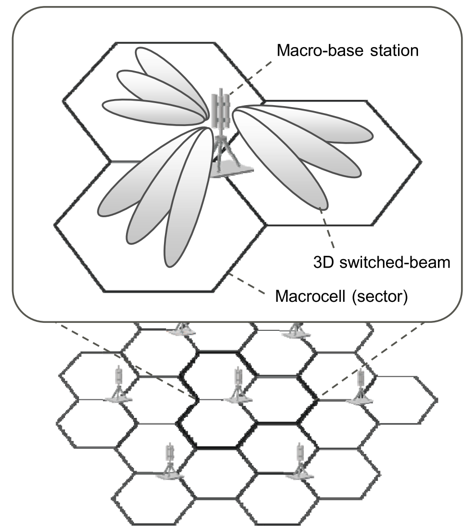

Fig. 1 Multi-cell structure for the proposed ICIC scheme.

Table 1 Simulation parameters.

Parameters	Settings
Cell layout	3 sectors × 7 cell sites
Inter-site distance (ISD)	500 m
System bandwidth	10 MHz
Transmission power	46 dBm
Antenna gain	BS: 14 dBi, UE: 0 dBi
Shadowing standard deviation	8 dB
Shadowing correlation	0.5 (site), 1.0 (sector) Correlation distance: 50 m
UE distribution	10, 30 UEs/sector Uniform distribution (8 drops)
Minimum UE distance from BS	35 m
BS antenna pattern (horizontal)	$A_H(\varphi) = -min\left[12\left(\frac{\varphi - \varphi_{azimuth}}{\varphi_{3dB}}\right)^2, A_m\right]$ $A_m = 25$ dB
BS antenna pattern (vertical)	$A_V(\theta) = -min\left[12\left(\frac{\theta - \theta_{tilt}}{\theta_{3dB}}\right)^2, SLA_v\right]$ $\theta_{3dB} = 10$ deg., $SLA_v = 20$ dB
BS antenna pattern (3D)	$A(\varphi,\theta) = -\min\{-[A_H(\varphi) + A_V(\theta)], A_m\}$
UE antenna pattern	Omni directional
Antenna height	BS: 32 m, UE: 1.5 m
Penetration loss	20 dB
Noise figure	9 dB
Pathloss	128.1 + 37.6log(d) d: Distance in kilometers
Fading model	Flat Rayleigh fading (Independent for each band)
Traffic model	Full buffer
Scheduling	Throughput-based PF

$$\gamma_{n,k}^{j} = \frac{A_{n,j,k} P_{j,k} G_{n,j,k}}{\sum_{i=1, i\neq j}^{N_{cell}} A_{n,i,k} P_{i,k} G_{n,i,k} + N_0}, \tag{1}$$

where $A_{n,j,k}$ and $G_{n,j,k}$ correspond to the antenna gain and the channel gain including pathloss and shadowing, respectively. $P_{j,k}$ corresponds to the transmission power in band #k of macrocell #j. N_{cell} is the number of macrocells and N_0 is the thermal noise power including the noise figure. Since we deal with the downlink and the traffic model of full buffer, the inter-cell interference level is not affected by user scheduling. We also assume that the antenna pattern is set for each band and not dynamically changed. The index of macrocell #j is omitted for simplicity, and the SINR $\gamma_{n,k}^{j}$ will simply be expressed as $\gamma_{n,k}$. The throughput of each UE is calculated assuming throughput-based PF scheduling, which selects the UE with maximum PF metric $\Gamma_{n,k}$, given as

$$\Gamma_{n,k} = \frac{R_{n,k}}{\tilde{R}_n}, \tag{2}$$

where $R_{n,k}$ is the achievable instantaneous throughput and $\tilde{R}_n$ is the averaged throughput of UE #n over the time and frequency bands. $R_{n,k}$ is calculated as

$$R_{n,k} = W_k \cdot \min\left\{8.33, \log_2\left(1 + \frac{\gamma_{n,k}}{\alpha}\right)\right\}, \tag{3}$$

where W_k is the bandwidth of band #k. α is the system efficiency factor, and it is set to 3 dB in the simulation. $R_{n,k} = 8.33$ [bps/Hz] corresponds to the maximum spectrum efficiency of LTE assuming 2×2 MIMO [14]. Note that the SINR $\gamma_{n,k}$ is assumed to be ideally estimated and we do not consider the delay in the estimation.

2.2 Conventional FFR

Figure 2 outlines the frequency and power allocation of the conventional FFR. Its performance is evaluated in order to compare it with our centralized ICIC scheme. The scheme in Fig. 2 is called soft frequency reuse (SFR) [15]. In SFR, the system bandwidth is divided into three equal bands, where the transmission power of one of the bands is set higher than the rest. This band is called the "cell-edge user band" and it is assigned to users situated around the cell border. The positions of the cell-edge user band are coordinated so as to reduce inter-cell interference, as shown in Fig. 2. The horizontal beamwidth φ_{3dB} is set to 70 degrees, same as the conventional macrocell. The transmission power of cell-edge user band is set 9 dB higher than the rest. The antenna down tilt is adjusted to improve the performance of the conventional FFR. Here, θ_{tilt} of the cell-edge user band is set to 11 degrees, while that of the other bands is set to 17 degrees. These parameters are chosen to give the best performance in our simulation. In general, UEs are categorized as cell-center users or cell-edge users [16]. However, we do not restrict the UE assignment depending on the geographic location of UEs. As described in [11], the UE assignment to frequency resources is calculated by solving the PF utility maximization problem. This means PF scheduling automatically assigns UEs to a suitable band that is a cell-edge user band or cell-center user band on the basis of the PF metric calculated by Eq. (2). As a result, the cell-edge user throughput improves.

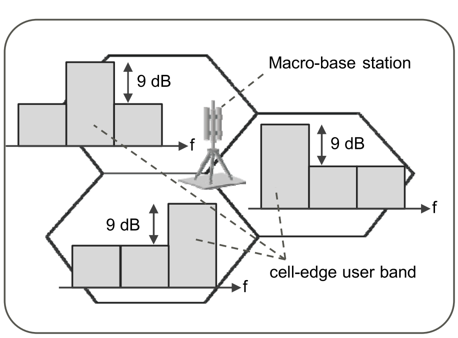

Fig. 2 Frequency and power allocation for conventional FFR.

2.3 Proposed ICIC Using 3D Beam-Switching

The system configuration of our scheme with multi-band 3D beam-switching is outlined in Figs. 3 and 4. Each band of each sector has a capability to transmit a signal via narrow beam, where φ_{3dB} is set narrower than the conventional sector antenna. The azimuth angle $\varphi_{azimuth}$ of the narrow beam can be switched in nine steps, i.e., −53.3, −40.0, −26.7, −13.3, 0.0, 13.3, 26.7, 40.0, and 53.3 degrees, and the down tilt θ_{tilt} in four steps, i.e., 11, 13, 15, and 17 degrees. Here, the choice of steps is an example, but it considers the trade-off between complexity and performance. In total, the simulation has 36 different narrow beam patterns. The horizontal beamwidth φ_{3dB} of the narrow beam is one of the parameters, and its effect is evaluated. Note that the antenna gain is fixed at 14 dBi for every beamwidth described in this paper, because the simulation setting of ISD=500 m results in interference-limited condition and the antenna gain does not have a big influence on the throughput. The transmission power of each band is set equal since we evaluate the effect of ICIC by controlling the direction of narrow 3D beams in this paper.

Moreover, our centralized ICIC scheme can execute spatial user multiplexing by assigning up to two different narrow beams to the same frequency band. Since two UEs can transmit simultaneously by using two different beams in the same band, it is expected that the total throughput will greatly improve. In this paper, we evaluate throughput performance for cases with and without spatial user multiplexing. Note that MIMO signal processing is not considered for the reception in case of the spatial user multiplexing and the user throughput is calculated by Eq. (3).

The centralized controller collects the received signal strength of all UEs connected to the controlled base stations. The UE measures the received signal strength for all beams of adjacent cells by detecting the orthogonal reference signal of each beam and feeds them back to the connected base sta-

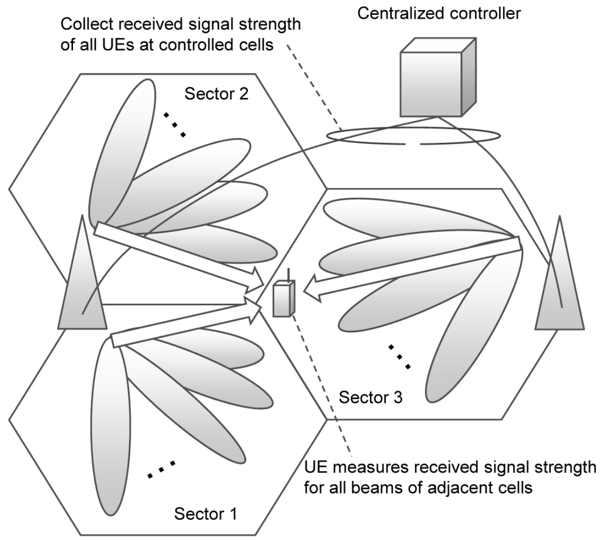

Fig. 3 System configuration for the proposed ICIC scheme.

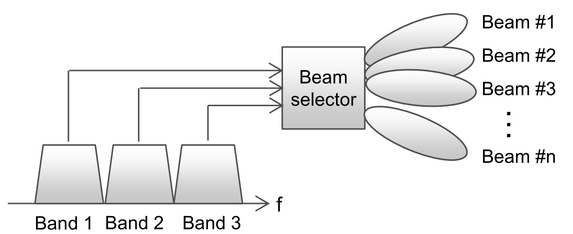

Fig. 4 Beam selection of proposed multi-band 3D beam-switching.

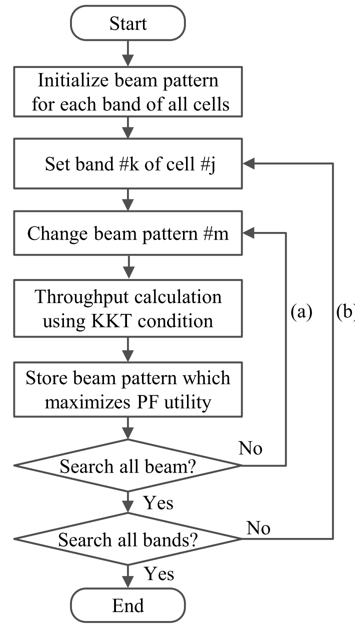

Fig. 5 Algorithm of the proposed scheme.

tion in the case of FDD. In a TDD system, it is possible for a base station to estimate the received signal strength of each UE by receiving the uplink reference signal using the same beam pattern as the downlink. As an alternative, UEs can report their geographical locations measured by the global positioning system (GPS), and the centralized controller can calculate the received signal strength of each UE by using a propagation simulation technique, such as ray tracing.

The 3D beam-switching selects a beam pattern for each frequency band, as shown in Fig. 4. The received signal strength reported to the centralized controller is the long-term mean value in which fast fading has been averaged out. After 3D beam patterns of all bands are selected by the proposed ICIC scheme, the user throughput evaluation is carried out assuming the independent flat Rayleigh fading for each band.

3. Algorithm

This section describes the algorithm that searches the sub-optimum beam patterns under criteria that maximize the PF utility. This section also explains our throughput calculation method applying the KKT condition.

3.1 Sub-Optimum Search Algorithm

The centralized controller decides the beam pattern for each band of all macrocells by utilizing the collected received signal strength information. The computation time would be prohibitive if we calculated all possible combinations of beam patterns, so instead, we execute the sub-optimum algorithm shown in Fig. 5.

First, the beam patterns are initialized for each band of all cells. The initial value of the down tilt θ_{tilt} is 15 degrees, and the azimuth angle $\varphi_{azimuth}$ is selected from among nine azimuth candidates (see Sect. 2.3) so that multiple beams in multiple bands equally cover the whole sector. For example, in the case of a three-band configuration, $\varphi_{azimuth}$ is set to −26.7 degrees for band #1, 0 degrees for band #2, and 40 degrees for band #3. When two beams are assigned to the same band, $\varphi_{azimuth}$ is set to −26.7 and 26.7 degrees for band #1, 0 and 53.3 degrees for band #2, and 40 and −26.7 degrees for band #3. Second, a band is chosen from among the bands of all macrocells, and band $\#k$ of macrocell $\#j$ is set for the next step. Third, the beam pattern is chosen from all beam patterns with different azimuth and tilt angles. Fourth, the throughputs of all UEs are calculated using KKT condition, as explained in the next subsection. Fifth, the beam pattern giving the larger PF utility is recorded in order to find the beam pattern that maximizes the PF utility. The number of loops (a) is 36, which is equivalent to the number of beam patterns. In the case of spatial user multiplexing, the number of loops (a) is 72, because we assume multiplexing of a maximum of two users. The number of loops (b) is 63 in the case of the system having seven cell sites with three sectors per site and three bands per sector.

Figure 6 is the additional procedure for the case of spatial user multiplexing. This algorithm is carried out after the procedure in Fig. 5, and it checks if PF utility improves when either beam is turned off. As a result, the one beam and two beams assignments are mixed in the case of spatial

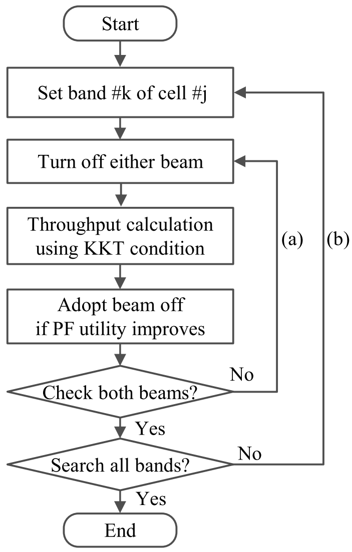

Fig. 6 Additional procedure in the case of spatial user multiplexing.

user multiplexing.

The criteria that maximizes PF utility is used to decide the sub-optimum beam patterns because this criteria takes into consideration both user throughput and fairness. However, other criteria, such as average user throughput, minimum user throughput, and fairness, can be used depending on the operation policy of the system.

3.2 Throughput Calculation using KKT Condition

This subsection explains how we calculate user throughput and PF utility using the KKT condition. The achievable instantaneous throughput $R_{n,k}$ is calculated using Eq. (3). $R_{n,k}$ is the expected throughput when UE #n is assigned to band #k by the connected base station. Since this throughput calculation is carried out at the centralized controller based on the UE measurement, pathloss and shadowing are considered, but fast fading is not considered.

We will now introduce the resource allocation ratio $p_{n,k}$ [11], which corresponds to the assignment ratio of band #k to UE #n. We can express the throughput of UE #n after scheduling as

$$T_n = \sum_{k=1}^{N_{band}} p_{n,k} R_{n,k} \quad (n = 1, \ldots, N_{UE}), \tag{4}$$

where N_{band} is the number of bands in each macrocell and N_{UE} is the number of UEs managed by the centralized controller. Accordingly, the PF utility maximization problem is expressed as

$$\begin{aligned} &\mathit{maximize} \;\; U = \sum_{n=1}^{N_{UE}} \log\left(\sum_{k=1}^{N_{band}} p_{n,k} R_{n,k}\right) \\ &\mathit{subject\ to} \;\; \sum_{n=1}^{N_{UE}} p_{n,k} = 1, \;\; p_{n,k} \geq 0 \quad (k = 1, \cdots, N_{band}), \end{aligned} \tag{5}$$

where U is the definition of PF utility. Equation (5) is a narrowly defined convex function [17], and the set of $p_{n,k}$ that maximizes U can be derived from the KKT condition [11]. The solution is expressed as

$$\begin{aligned} &\sum_{n=1}^{N_{UE}} \max\left\{0, \frac{1}{\mu_k} - \frac{T'_{n,k}}{R_{n,k}}\right\} = 1 \quad (k = 1, \cdots, N_{band}) \\ &T'_{n,k} = \sum_{i=1, i\neq k}^{N_{band}} p_{n,i} R_{n,i}, \end{aligned} \tag{6}$$

where μ_k is the Lagrange multiplier for the equality constraint of Eq. (5). Equation (6) can be solved by the water-filling algorithm [17] and the optimum set of $p_{n,k}$ can be obtained. We start with the initial value of $p_{n,k}$ (e.g., $p_{n,k} = 1/N_{UE}$) for all bands. Then, we recalculate the $p_{n,k}$ of each band by solving Eq. (6) with the water-filling algorithm. We iterate this recalculation procedure twenty times for convergence. Note that the PF utility monotonically increases with each iteration. Finally, the user throughput T_n can be obtained by substituting $p_{n,k}$ into Eq. (4).

4. Performance Evaluation

Computer simulations were carried out to evaluate the performance of our proposed scheme. Here, we first show the basic throughput performance of our scheme, showing the effect of varying the number of bands, beamwidth, and angle spread, in comparison with the conventional macrocell and the conventional FFR. After that, we assess the feasibility of our scheme by investigating the effect of a measurement threshold, user mobility, and the existence of uncontrolled base stations.

4.1 Basic Throughput Performance

Figure 7 plots the simulated user throughput with the proposed scheme, conventional macrocell, and conventional FFR for 10 UEs per macrocell, and Fig. 8 plots them for 30 UEs per macrocell. The proposed scheme without spatial user multiplexing is plotted as “Mux 1” and with spatial

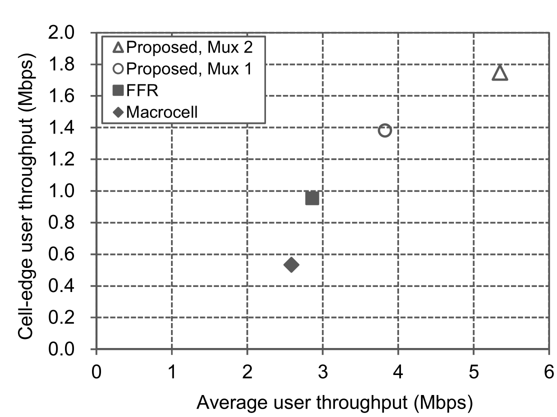

Fig. 7 User throughput comparison (10 UEs/macrocell).

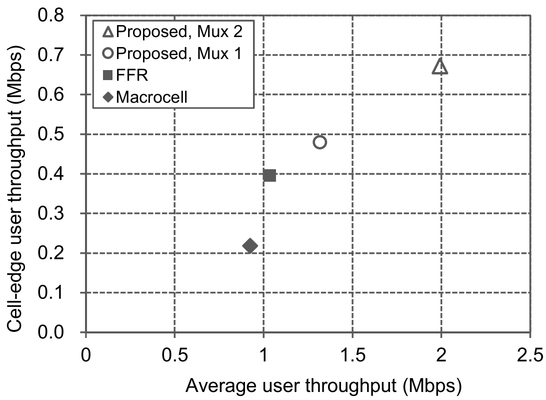

Fig. 8 User throughput comparison (30 UEs/macrocell).

user multiplexing as "Mux 2". The parameters shown in Table 1 are used in this simulation. The number of bands is set to four except in the case of FFR which has three bands, as shown in Fig. 2. The multipath model has five dominant paths at the base station antenna, and each path has independent Rayleigh fading. We assume that the horizontal angle spread obeys a Laplace distribution [18] and that there is no vertical angle spread. The angle spread is set to the standard deviation of 5 degrees, and the beamwidth for the proposed scheme is set to 30 degrees. The horizontal axis in Figs. 7 and 8 is the average user throughput, and the vertical axis is the cell-edge user throughput that corresponds to a 5% CDF throughput of all UEs. The results show that compared with the conventional macrocell in the case of 10 UEs per macrocell, the proposed scheme achieves about 1.5 times higher average user throughput and about 2.6 times higher cell-edge user throughput without spatial user multiplexing, and about 2.1 times higher average user throughput and about 3.3 times higher cell-edge user throughput with spatial user multiplexing. Similar gains are observed for the case of 30 UEs per macrocell.

Figures 9 and 10 plot the throughput of the proposed scheme as a function of the number of bands for 10 UEs per macrocell and an angle spread of 5 degrees. Figure 9 plots the average user throughput, and Fig. 10 plots the cell-edge user throughput. Throughput for beamwidths of 10 degrees and 30 degrees are plotted for cases with and without spatial user multiplexing. As the number of bands increases, both the average and cell-edge user throughputs improve because the narrow beam is assigned to each band and sufficient coverage can be achieved by a larger number of beams. The results show that more than four bands are necessary to achieve sufficient throughput in the case of a 30-degree beamwidth and more than five bands are necessary for the 10-degree beamwidth. Thus, we use a four-band configuration in the following simulations.

Figures 11 and 12 show the effect of changing the beamwidth for the case of 10 UEs per macrocell and the four-band configuration. Figure 11 plots the average user throughput, and Fig. 12 plots the cell-edge user throughput. Throughputs for a 5-degree angle spread and 20-degree an-

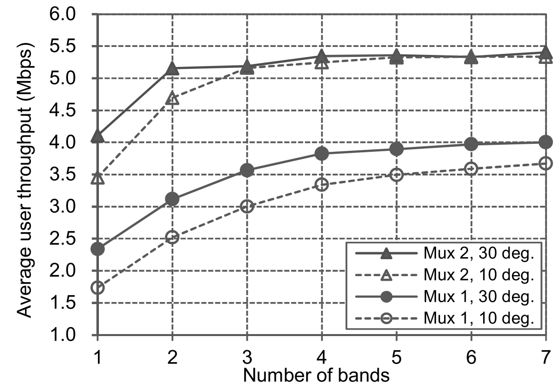

Fig. 9 Effect of number of bands (average user throughput).

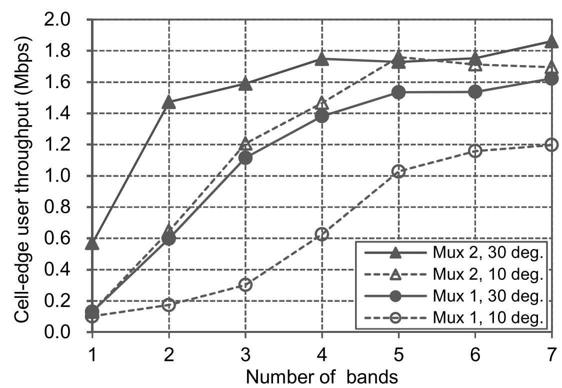

Fig. 10 Effect of number of bands (cell-edge user throughput).

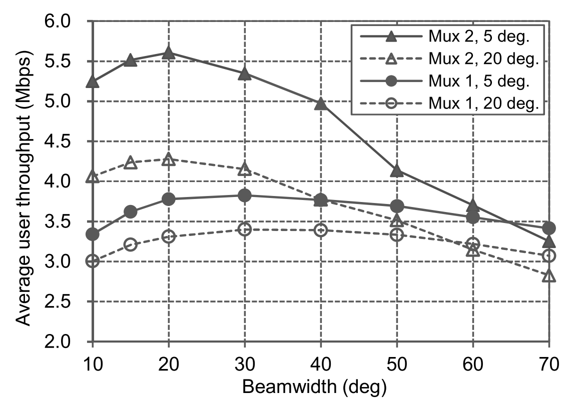

Fig. 11 Effect of changing the beamwidth (average user throughput).

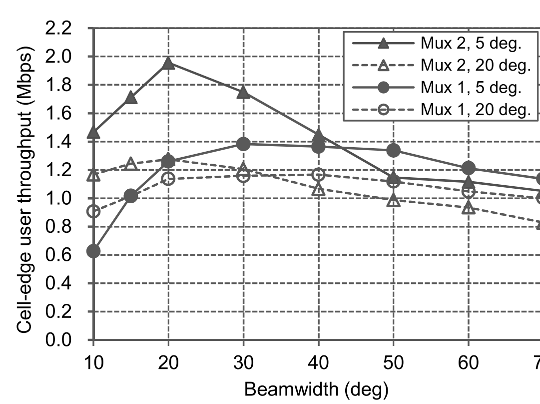

Fig. 12 Effect of changing the beamwidth (cell-edge user throughput).

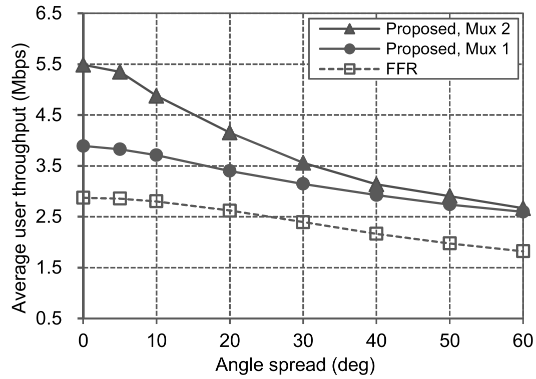

Fig. 13 Effect of angle spread (average user throughput).

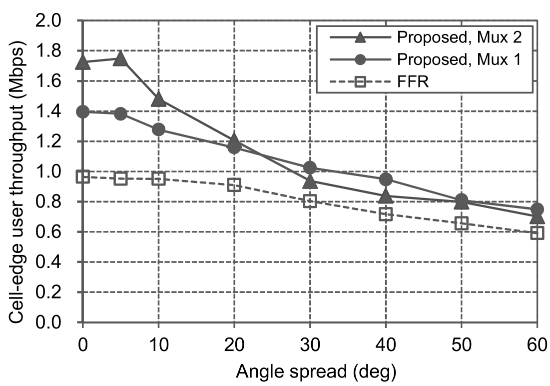

Fig. 14 Effect of angle spread (cell-edge user throughput).

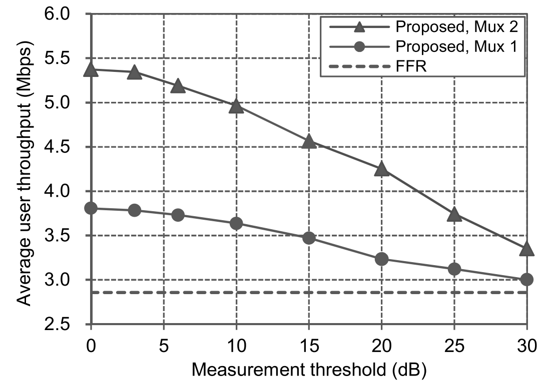

Fig. 15 Effect of measurement threshold (average user throughput).

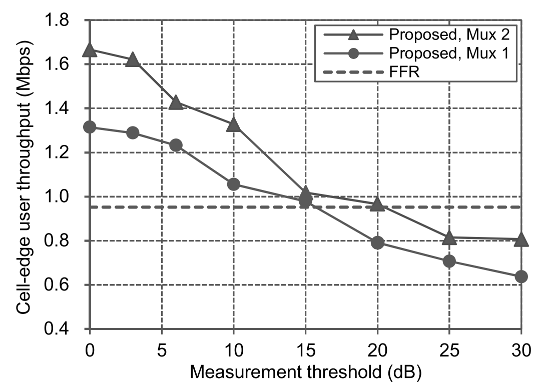

Fig. 16 Effect of measurement threshold (cell-edge user throughput).

gle spread are plotted for cases with and without spatial user multiplexing. The results show that the beamwidth of 30 degrees has the best throughput in the case without spatial user multiplexing, while that of 20 degrees has the best performance in the case with spatial user multiplexing. In the case of spatial user multiplexing, a narrower beamwidth can better reduce inter-cell interference as well as inter-beam interference. However, a beamwidth narrower than 20 degrees degrades coverage as well as throughput.

Figures 13 and 14 show the effect of the angle spread for the proposed scheme and the conventional FFR in the case of 10 UEs per macrocell. The proposed scheme assumes a 30-degree beamwidth and a four-band configuration. Throughputs for cases with and without spatial user multiplexing are plotted. Figure 13 plots the average user throughput, and Fig. 14 plots the cell-edge user throughput. As the angle spread increases, throughputs deteriorate for both the proposed scheme and the conventional FFR, because the angle spread reduces the desired signal power more than the inter-cell interference. Throughput in the case of spatial user multiplexing deteriorates faster than in the case without spatial user multiplexing because the number of bands assigned two beams at the same frequency band decreases due to the rise in inter-beam interference. The results show that an angle spread of less than 20 degrees is preferable in order to achieve a sufficient throughput gain under these simulation conditions. It is reported [18] that the Laplacian function matches the estimated power angle spread and a median angle spread of 5 degrees was observed for a 32 m antenna height. The feasibility study described in the next subsection therefore assumes an angle spread of 5 degrees.

4.2 Feasibility Study

The previous subsection assumed that all UEs ideally measure the received signal power of all bands for a total of 21 macrocells. Figures 15 and 16 plot the average and the cell-edge user throughput under the assumption that the UEs only measure the received signal power of base stations whose received signal power is more than a threshold. Here, we assume that the UEs detect the reference signal transmitted via the conventional sector antennas of the surrounding base stations and decide if they will measure and report the received signal power of each beam. Throughputs for a 5-degree angle spread, 30-degree beamwidth, four-band configuration, and 10 UEs per macrocell are plotted for cases with and without spatial user multiplexing. The horizontal axis is the threshold value, and the received signal-to-thermal noise power ratio (SNR) is taken as the measurement threshold. The performance of the conventional FFR is also plotted for comparison. The results show that a measurement threshold less than 3 dB is necessary to achieve sufficient gain for the proposed scheme. It is sufficient for

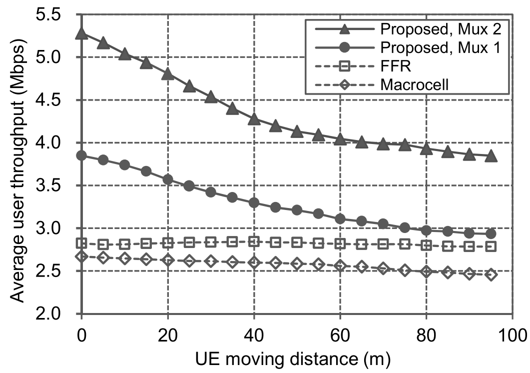

Fig. 17 Effect of UE motion (average user throughput).

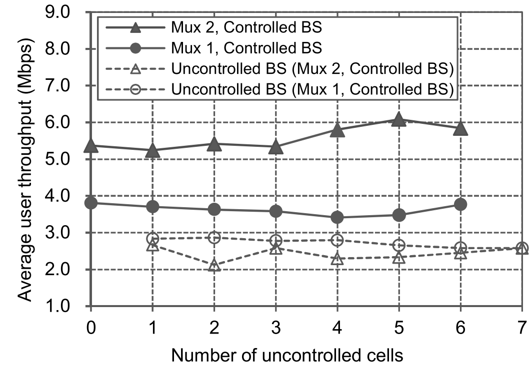

Fig. 19 Effect of uncontrolled cells (average user throughput).

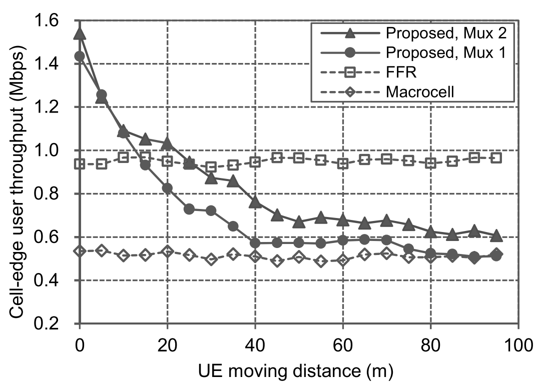

Fig. 18 Effect of UE motion (cell-edge user throughput).

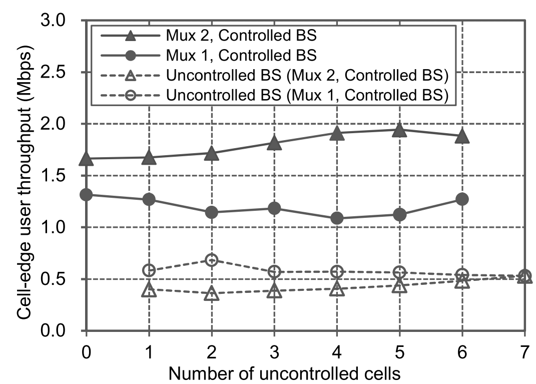

Fig. 20 Effect of uncontrolled cells (cell-edge user throughput).

the UE to measure the signal whose SNR is more than 0 dB. The analysis of this simulation shows that UEs measure about 7.5 and 5.8 macrocells among 21 macrocells for 0 dB and 3 dB measurement thresholds, respectively.

An actual mobile system would need to account for the motion of the UE during or after the decision about the sub-optimum beam patterns. The simulation thus shows how the throughput changes along with motion of the UE after the beam patterns had been decided, and investigates the period for updating beam patterns. We assume that all UEs move in straight lines in random directions at the same speed. The UE continues to move through 21 macrocells because the simulation uses a wrap-around technique. A correlation distance of 50 m [19] is assumed so that the shadowing depends on the location of the UE. Figures 17 and 18 plot the average user throughput and the cell-edge user throughput for the proposed scheme with and without spatial user multiplexing, the conventional macrocell, and the conventional FFR in the case of 10 UEs per macrocell. An angle spread of 5 degrees is assumed for all schemes. The proposed scheme uses a 30-degree beamwidth, a four-band configuration, and a measurement threshold of 0 dB, while the conventional FFR uses a 70-degree beamwidth and a three-band configuration, whereas the conventional macrocell has a 70-degree beamwidth and a four-band configuration. The results show that the average user throughput gradually decreases because of the motion of the UEs, but the proposed scheme still maintains a gain over both the conventional FFR and the conventional macrocell. However, the cell-edge user throughput of the proposed scheme rapidly decreases. In the case of a UE moving over 20 m, the cell-edge user throughput of the proposed scheme becomes worse than that of the conventional FFR. In order to achieve better cell-edge user throughput than the conventional FFR, the beam patterns should be updated before all UEs move 20 m, and to achieve a better average user throughput than the conventional FFR, the beam patterns should be updated before all UEs move about 60 m. If we assume the UE moves at 3.6 km/h, i.e., walking speed, the beam patterns should be updated every 20 sec to achieve higher cell-edge user throughput, and the beam patterns should be updated every 60 sec to achieve higher average user throughput. Although the performance depends on the simulation conditions and how the UE moves, it can be said that the proposed scheme which uses only narrow beams is vulnerable to user mobility. Hence, it is presumable that applying wide beams in addition to narrow beams might be effective in avoiding severe degradations in cell-edge user throughput due to user mobility.

The last feasibility study is on the effect of uncontrolled cells. The existence of uncontrolled cells should be considered in an actual cellular system. It is conceivable that uncontrolled base stations which do not have a beam-switching capability exist inside the centralized controlled area, and that other uncontrolled cells exist around its border. A realistic solution is to establish autonomous ICIC between the controlled and uncontrolled cells by using the X2-interface [6]. However, an algorithm that combines centralized ICIC and autonomous ICIC is left as a future study. Hence, here, we simply evaluate the effect of uncontrolled cells among the controlled cells by randomly choosing cell sites and making them uncontrolled. Figures 19 and 20 plot the average and cell-edge user throughput in the case of a 5-degree angle spread, a four-band configuration, and 10 UEs per macrocell. The throughput of both controlled and uncontrolled base stations are plotted. We assume a 30-degree beamwidth and 0-dB measurement threshold for the controlled base station and a 70-degree beamwidth for the uncontrolled base station. Spatial user multiplexing is applied to only the controlled base station. The horizontal axis is the number of uncontrolled cells. For example, if the number of uncontrolled cells is three, the number of controlled cells becomes four in this simulation assuming the total seven cell sites. The results show that the uncontrolled cells does not degrade the throughput of the controlled cells because increasing the number of uncontrolled cells, i.e., decreasing the number of controlled cells, allows more freedom for controlling narrow beams and improves the throughput of controlled cells. The throughput of uncontrolled cells is degraded by applying the spatial user multiplexing to controlled cells because the controlled base station using two beams per band increases the interference affecting uncontrolled cells.

5. Conclusions

We proposed a novel centralized ICIC scheme using multi-band 3D beam-switching and demonstrated that it significantly improves both the average and cell-edge user throughput in comparison with the conventional FFR and conventional macrocell schemes. Our scheme uses a centralized controller that coordinates the directions of the narrow beams of each band. It can realize spatial user multiplexing by assigning up to two narrow beams to the same frequency band. We developed an algorithm for the centralized controller to calculate sub-optimum combinations of the narrow beams so as to maximize the PF utility. The results of simulations confirm that the proposed scheme without user multiplexing achieves about 1.5 times higher average user throughput and about 2.6 times higher cell-edge user throughput compared with the conventional macrocell. Moreover, with spatial user multiplexing, it achieves about 2.1 times higher average user throughput and about 3.3 times higher cell-edge user throughput. We also carried out various simulations to confirm the throughput performance and the feasibility of our proposed centralized ICIC scheme. Since the proposed scheme using narrow beams is sensitive to user mobility, it is more suited to low-mobility environments.

References

[1] Cisco Visual Networking Index: Forecast and Methodology, 2013–2018, June 2014.

[2] T. Nakamura, "Views on IMT beyond 2020," ITU-R Working Party 5D Workshop, Feb. 2014.

[3] S.H. Ali and V.C.M. Leung, "Dynamic frequency allocation in fractional frequency reused OFDMA networks," IEEE Trans. Wireless Commun., vol.8, no.8, pp.4286–4295, Aug. 2009.

[4] M. Rahman and H. Yanikomeroglu, "Enhancing cell-edge performance: A downlink dynamic interference avoidance scheme with inter-cell coordination," IEEE Trans. Wireless Commun., vol.9, no.4, pp.1414–1425, April 2010.

[5] D. Kimura, Y. Harada, and H. Seki, "De-centralized dynamic ICIC using X2 interfaces for downlink LTE systems," Proc. IEEE Vehicular Technology Conference (VTC Spring), pp.1–5, May 2011.

[6] 3GPP, TS 36.423 (V11.8.0) "Evolved universal terrestrial radio access network (E-UTRAN); X2 application protocol (X2AP)," March 2014.

[7] P. Chaipanya, P. Uthansakul, and M. Uthansakul, "Reduction of inter-cell interference using vertical beamforming scheme for fractional frequency reuse technique," Proc. Asia-Pacific Microwave Conference (APMC), pp.1614–1617, Dec. 2011.

[8] Y. Li, X. Ji, M. Peng, Y. Li, and C. Huang, "An enhanced beamforming algorithm for three dimensional MIMO in LTE-advanced networks," Proc. International Conference on Wireless Communications & Signal Processing (WCSP), pp.1–5, Oct. 2013.

[9] Y.-S. Cheng and C.-H. Chen, "A novel 3D beamforming scheme for LTE-Advanced system," Proc. Asia-Pacific Network Operations and Management Symposium (APNOMS), pp.1–6, Sept. 2014.

[10] C.-S. Lee, M.-C. Lee, C.-J. Huang, and T.-S. Lee, "Sectorization with beam pattern design using 3D beamforming techniques," Proc. Asia-Pacific Signal and Information Processing Association Annual Summit and Conference (APSIPA), Oct.-Nov. pp.1–5, 2013.

[11] H. Seki, T. Kobayashi, and D. Kimura, "Selection of component carriers using centralized baseband pooling for LTE-advanced heterogeneous networks," IEICE Trans. Commun., vol.E96-B, no.6, pp.1288–1296, June 2013.

[12] F. Sallabi, A. Lakas, K. Shuaib, and M. Boulmalf, "WCDMA downlink simulator with efficient wrap-around technique," Proc. IEEE and IFIP Wireless and Optical Communications Networks (WOCN), pp.472–476, March 2005.

[13] 3GPP, TR 36.814 (V9.0.0), "Further advancements for E-UTRA physical layer aspects," March 2010.

[14] 3GPP, TS 36.213 (V9.3.0), "Evolved universal terrestrial radio access (E-UTRA); Physical layer procedures (Release 9)," Sept. 2010.

[15] R1-050507, "Soft frequency reuse scheme for UTRAN LTE," 3GPP RAN WG1#41, Athens, Greece, May 2005.

[16] D. Lee, G.Y. Li, and S. Tang, "Intercell interference coordination for LTE systems," IEEE Trans. Veh. Technol., vol.62, no.9, pp.4408–4420, Nov. 2013.

[17] S. Boyed and L. Vandenberghe, Convex Optimization, Cambridge University Press, 2004.

[18] K.I. Pedersen, P.E. Mogensen, and B.H. Fleury, "A stochastic model of the temporal and azimuthal dispersion seen at the base station in outdoor propagation environments," IEEE Trans. Veh. Technol., vol.49, no.2, pp.437–447, March 2000.

[19] IEEE 802.16m-08/004r4, "IEEE 802.16m Evaluation Methodology Document (EMD)," Nov. 2008.

Hiroyuki Seki received the B.E. degree from Waseda University, Tokyo, Japan in 1990 and the M.E. degree from Tokyo Institute of Technology in 1992. He joined Fujitsu Laboratories Ltd., Kanagawa, Japan in 1992, where he has been engaged in research and development of radio access technologies for 3G and 4G mobile systems. From 1999 to 2000, he stayed at Stanford University as a visiting scholar to study on smart antenna technology. He is currently a research manager at Network Systems Laboratories of Fujitsu Laboratories Ltd. His research interest also includes cognitive radio for future wireless systems. He is a co-recipient of the Best Paper Award of the 76th IEEE Vehicular Technology Conference. He is a senior member of IEEE.

Fumiyuki Adachi received the B.S. and Dr. Eng. degrees in electrical engineering from Tohoku University, Sendai, Japan, in 1973 and 1984, respectively. In April 1973, he joined the Electrical Communications Laboratories of Nippon Telegraph & Telephone Corporation (now NTT) and conducted various types of research related to digital cellular mobile communications. From July 1992 to December 1999, he was with NTT Mobile Communications Network, Inc. (now NTT DoCoMo, Inc.), where he led a research group on wideband/broadband CDMA wireless access for IMT-2000 and beyond. Since January 2000, he has been with Tohoku University, Sendai, Japan, where he is a Professor of Communications Engineering at the Graduate School of Engineering. In 2011, he was appointed a Distinguished Professor. His research interest is in the areas of wireless signal processing and networking including broadband wireless access, equalization, transmit/receive antenna diversity, MIMO, adaptive transmission, channel coding, etc. From October 1984 to September 1985, he was a United Kingdom SERC Visiting Research Fellow in the Department of Electrical Engineering and Electronics at Liverpool University. Dr. Adachi is an IEEE Fellow and a VTS Distinguished Lecturer for 2011 to 2013. He was a co-recipient of the IEEE Vehicular Technology Transactions Best Paper of the Year Award 1980 and again 1990 and also a recipient of Avant Grade award 2000. He is a Fellow of IEICE and was a recipient of IEICE Achievement Award 2002 and a co-recipient of the IEICE Transactions Best Paper of the Year Award 1996, 1998 and again 2009. He was a recipient of Thomson Scientific Research Front Award 2004, Ericsson Telecommunications Award 2008, Telecom System Technology Award 2009, and Prime Minister Invention Prize 2010.